ChemPubSoc Europe

DOI: 10.1002/open.201800146

Open Access ChemistryOPEN Full Papers

Synthesis, Spectroscopic Characterization, and Time-Dependent DFT Calculations of 1-Methyl-5-phenyl-5*H*-pyrido[1,2-*a*]quinazoline-3,6-dione and Its Starting Precursor in Different Solvents

Nagwa M. M. Hamada*[a]

In this study, 2-mercapto-3-phenyl-2,3-dihydro-1*H*-quinazolin-4-one (**1**), which exists as a thiol and thione tautomer, was treated with acetylacetone to give the target compound, namely, 1-methyl-5-phenyl-5*H*-pyrido[1,2-*a*]quinazoline-3,6-dione (**2**). The spectroscopic data, including UV/Vis, IR, ^{1}H NMR, ^{13}C NMR, and mass data, of this compound were recorded. The molecular structures of the starting material (**1**) and the product (**2**) were optimized by using density functional theory (DFT) by employing the B3LYP exchange correlation with the 6-311G (d,p) and 6-31G++ (d,p) basis sets. The electronic spectra were determined based on time-dependent DFT calculations in three different solvents (i.e., chloroform, ethanol, and acetonitrile) starting from the same solvated run of the optimized geometry with the same two basis sets. The solvent effects were considered based on the polarizable continuum model (PCM), and the energetic behavior of the compounds and the total static dipole moment (μ) in different solvents were examined in the two basis sets; the results showed that the total energy of the compounds decreased upon increasing the polarity of the solvent. Time-dependent DFT calculations were performed to analyze the electronic transitions for various excited states that reproduced the experimental band observed in the UV/Vis spectrum. A study on the electronic properties, such as the HOMO and LUMO energies, was performed by the time-independent DFT approach. Using the gauge-independent atomic orbital method (GIAO), the ^{1}H NMR chemical shifts were calculated and correlated with the experimental ones. The computed results showed that the introduction of different dielectric media had a slight effect on the stability and reactivity of the title compound as well as on the Milliken atomic charges and the molecular geometry. Besides, the molecular electrostatic potential of target product **2** was evaluated in different solvents.

1. Introduction

Quinazolinones are multilateral nitrogen-containing heterocyclic compounds that occupy an important position in showing many types of biological and pharmacological activities.[1,2] The synthetic quinazoline ring is part of several antibiotics that are known to inhibit the growth of Gram-positive bacteria and that are also active against various transplantable tumors.[3] Many of them show analgesic,[4] antifungal, antibacterial,[5–7] anticancer, and anti-inflammatory activities.[8] As pesticides, they are used as insecticidal[9,10] and antiviral agents.[11] Earlier reports showed that the presence of alkyl/aryl/heteroaryl groups at the 2- and 3-positions of the quinazolinone ring was beneficial to anti-inflammatory and antimicrobial activity. In this regard, it was planned to synthesize some new derivatives of quinazolin-4-one. In recent years, density functional theory (DFT) has been popular for theoretical modeling,[12–18] and a survey of the literature revealed that DFT has great accuracy in reproducing the experimental values for the geometry, dipole moment, vibrational frequency, and so on. The use of density functional theory calculations to predict the molecular structures and the spectroscopic properties of organic compounds is of interest,[19–24] as the DFT method has been proven to give satisfactory results with regard to the experimental ones. From this point of view, the aim of the present work was to describe and characterize the molecular structure, electronic spectra, and chemical shifts of the studied compounds, both experimentally and theoretically.

In the experimental part of our study, we considered two possible tautomers of 2-mercapto-3-phenyl-2,3-dihydro-1*H*-quinazolin-4-one (**1**), namely, the thione and thiol forms. Starting from synthesized compound **1**, the target product, 1-methyl-5-phenyl-5*H*-pyrido[1,2-*a*]quinazoline-3,6-dione (**2**), was obtained. The compounds were prepared and characterized by electronic spectroscopy, FTIR spectroscopy, NMR spectroscopy, mass spectrometry, and elemental analysis methods. In the theoretical part of this study, the molecular structures of the synthe-

[a] *Dr. N. M. M. Hamada*
Chemistry Department, Faculty of Education
Alexandria University
Alexandria, 21526 (Egypt)
E-mail: nagwahamada2002@alexu.edu.eg

Supporting Information and the ORCID identification number(s) for the author(s) of this article can be found under: https://doi.org/10.1002/open.201800146.

© 2018 The Authors. Published by Wiley-VCH Verlag GmbH & Co. KGaA. This is an open access article under the terms of the Creative Commons Attribution-NonCommercial-NoDerivs License, which permits use and distribution in any medium, provided the original work is properly cited, the use is non-commercial and no modifications or adaptations are made.

sized compounds in the ground states were calculated by using density functional theory (DFT) (B3LYP) with the 6-311G(d,p) and 6-31++G(d,p) basis sets. Time-dependent (TD) DFT calculations were performed to analyze the electronic transitions for various excited states that reproduced the experimental bands observed in the UV/Vis spectrum. The highest occupied molecular orbital (HOMO), the lowest unoccupied molecular orbital (LUMO), and the Mulliken atomic charges of the studied molecules were calculated with the 6-311G(d,p) and 6-31++G(d,p) basis sets starting from the optimized geometries. Using the gauge-independent atomic orbital method, the ^{1}H NMR and ^{13}C NMR chemical shifts were calculated and correlated with the experimental chemical shifts. The theoretically obtained results were found to be consistent with the experimental data reported. The chemical reactivity and stability of **2** were explored based on the molecular electrostatic potential (MEP).

2. Results and Discussion

2.1. Chemistry

Our synthetic strategy utilizing the prepared quinazolinone derivative 2-mercapto-3-phenyl-2,3-dihydro-1*H*-quinazolin-4-one (**1**) afforded an unexpected one-pot synthesis of novel tricyclic product **2**. The first step in this reaction involved the reaction of the amino group in anthranilic acid with the thioxo group of phenylthiourea, and this was followed by nucleophilic attack of the nitrogen nucleophile at the carboxylic carbonyl group to produce compound **1** upon elimination of one molecule of ammonia (Scheme 1). The target molecule, 1-methyl-5-phenyl-5*H*-pyrido[1,2-*a*]quinazoline-3,6-dione (**2**), was obtained in good yield and excellent purity by nucleophilic attack of the electrons of the SH and NH groups of compound **1** on acetylacetone with ring closure and elimination of H_2S and H_2O.

The molecular structures of synthesized compound **1** and tricyclic quinazolinone product **2** were established by NMR

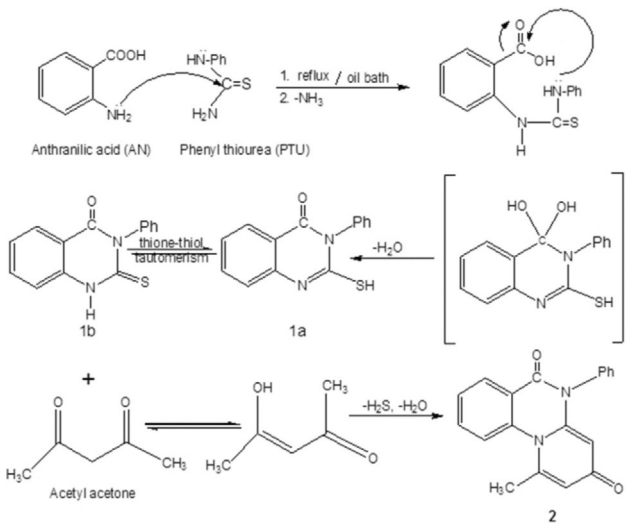

Scheme 1. Synthesis of quinazolinone derivatives **1** and **2**.

spectroscopy, IR spectroscopy, MS, elemental analysis, and melting points. Interestingly, the infrared spectrum of **1** showed the appearance of both C=S and S–H at $\tilde{\nu}=1268$ and 2924 cm^{-1}, which confirmed the existence of thione–thiol tautomerism. Moreover, the spectra of both compounds showed other characteristic bands at $\tilde{\nu}=3245$ (NH), 1661 (CO), 1621 (CN), and 1531 cm^{-1}(C=C). The expanded aromatic region of the ^{1}H NMR spectrum of **1** showed the presence of a multiplet at $\delta=6.64$–7.70 ppm corresponding to the nine aromatic protons of the phenyl and quinazolinone rings; furthermore, we observed extensive thiol–thione tautomerism due to the presence of the imino proton at $\delta=9.98$ ppm, which confirmed the thione structure, and a singlet at $\delta=5.45$ ppm corresponding to the thiol group, which confirmed the thiol form.[25,26] The infrared spectrum of newly synthesized quinazolinedione derivative **2** showed stretching vibrational bands at $\nu=1663$ (CO) and 1529 cm^{-1} (C=C). The^{1}H NMR spectrum showed the presence of two separate multiplets, one at $\delta=7.236$–7.499 ppm corresponding to the five aromatic protons of the N5 phenyl ring and another at $\delta=7.759$–7.7961 ppm corresponding to the four aromatic protons of the fused ring of the quinazolinone moiety. The spectrum also showed a singlet at $\delta=3.687$ ppm corresponding to the methyl group at C1 and another singlet at $\delta=2.510$ ppm corresponding to the two equivalent protons at C2 and C4.The mass spectrum of **2** showed no molecular ion signal, and additionally, it showed different fragments with different intensities that confirmed its structural formula (Scheme 2).

2.2. DFT Results

The tautomerism of organic compounds has been the subject of extensive theoretical studies by using different quantum-chemical methods.[27] DFT computational codes are used in practice to investigate the structural, magnetic, and electronic properties of molecules. The stability and chemical reactivity of these tautomers in the gas phase and in solution have been predicted by using the well-known quantum-chemical methods described above. However, DFT calculations produce the electron densities of molecules with good results and, thus, provide everything that is needed to determine the dipole moment with accuracy.

2.2.1. Total Optimization Energy Predictions

The relative stabilities and population of isomers **1a** and **1b** were predicted by using two basis sets, B3LYP/6311G(d,p) and 6-31++G(d,p), with two polarized basis functions, d and p; the presence of these two polarized functions is essential for adjusting the DFT analysis. One can conclude that novel 4-quinazolinone is more stable than anthranilic acid (AN) and phenylthiourea (PTU), which supports nucleophilic attack of the nitrogen atom of phenylthiourea at the carboxylic carbonyl group of anthranilic acid to obtain tautomers **1a** and **1b** (Figure 1).

The total optimization energies of PTU and AN reached −779.2519 and −467.7612 au, respectively (see Figure S1 in

© 2018 The Authors. Published by Wiley-VCH Verlag GmbH & Co. KGaA, Weinheim

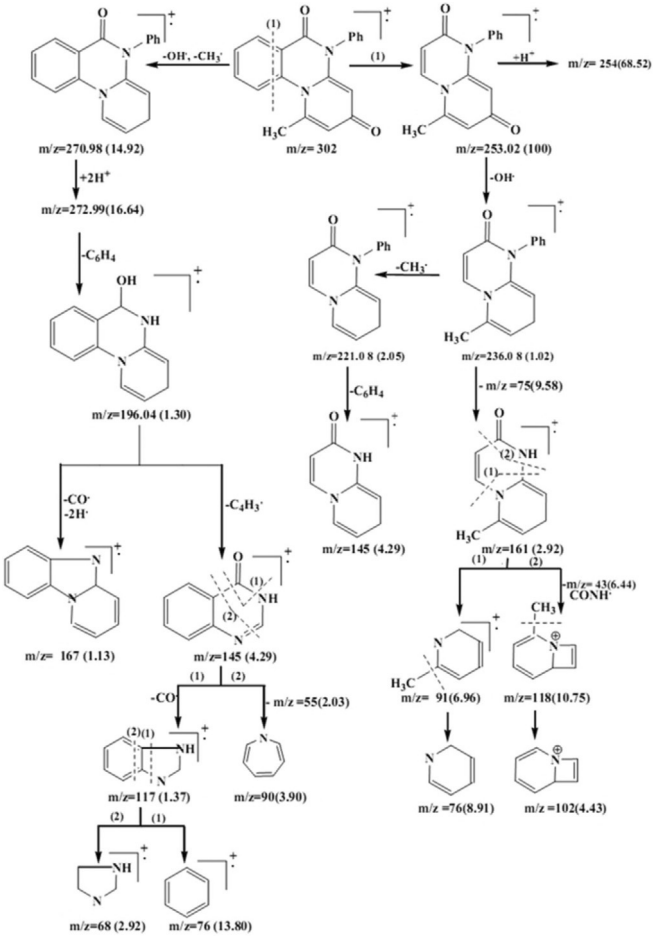

Scheme 2. Mass spectrum of targeted compound **2**.

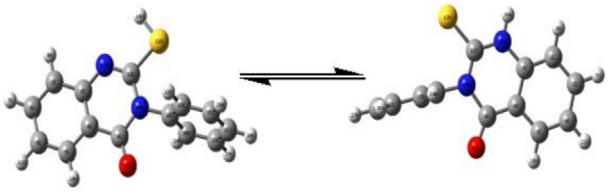

Figure 1. Equilibrium structures of the thiol and thione tautomers computed at the B3LYP/631++(d,p) level.

the Supporting Information). From the total optimized energies of the two tautomers at the B3LYP/6-311G(d,p) and B3LYP/6-31++G(d,p) levels, we confirmed that the thione tautomer (−1122.6683, −1122.5090 au, respectively) was more stable than the thiol tautomer (−1122.6538, −1122.1976 au, respectively) (Figure S2).

The calculations performed at the B3LYP/6-311G (d) and B3LYP/6-31++G (d,p) levels for target product quinazoline dione **2** showed that the DFT-obtained total optimization energy was greater for the 6-311G basis set (−992.4286 au) than for the 6-31++G basis set (−992.4686 au) (Figure S3). Consequently, the stability of synthesized compound **2** is affected by the basis set (Figure 2).

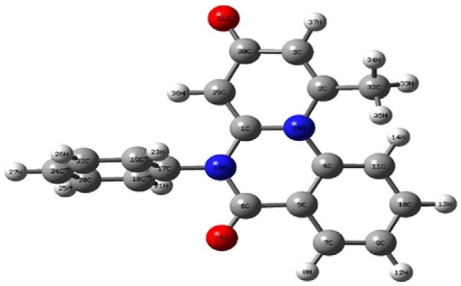

Figure 2. Optimized structure of quinazoline dione **2** computed at the B3LYP/6-31++G(d,p) level.

2.2.1.1. Energies and Dipole Moments

The dipole moment, an important factor in measuring the effects of various solvents with different dielectric constants, gives rise to strong solvent-polarity effects.[28–30] Solvent effects improve the delocalization of charges in molecules and, therefore, cause the dipole moments to increase, which causes reorientation of the solvent molecules to produce a large reaction field. Experimentally, the UV/Vis spectrum of **1** was recorded in different solvents with different dielectric constant (ε) values [chloroform (nonpolar), $\varepsilon = 4.81$; ethanol (polar, protic), $\varepsilon = 24.85$; and acetonitrile (polar, aprotic), $\varepsilon = 37.5$] at room temperature to evaluate the total energies and dipole moments in different solvent media. The time-dependent self-consistent field (TD-SCF) method was used for the structures optimized with the 6-311G and 6-31++G basis sets to analyze synthesized quinazolinone derivatives **1a**, **1b**, and **2** in chloroform, ethanol, and acetonitrile as a means to investigate their stability and reactivity and to assess how the set of computational parameters in TD-DFT affected the dipole moment values and excitation energies.

The molecular dipole moment (μ) values and the total energies (Hartree) in the gas phase and in different solvents calculated at the two basis sets are listed in Table S1. One can conclude from the data that the dipole moment values of the studied compounds are clearly affected by two factors: basis-set effects and solvent effects. From the dipole moments calculated for tautomers **1a** and **1b**, it was found that the dipole moments of both tautomers increased on going from the gas phase to the solvent phase, depending on the dielectric constant of the solvent used. Calculations performed by using the 6-31++ G basis set, which gives more logically accurate results, showed that the dipole moment of **1b** was greater than that of tautomer **1a** and that this value increased upon increasing the polarity of the solvent used. Furthermore, from Table S1, the dipole moment of target product **2** varies from 5.1575 to 7.4894 D on going from the gas phase to the solvent acetonitrile; thus, in different media, the solvent polarity increases the dipole moment of **2**, which gives an idea about the geometry and charge distribution within the molecular system, and the solvent polarity also affects the reactivity and stability of **2**. However, we can conclude that although the dipole moments increases, the total molecular energy obtained by the polarizable continuum model (PCM) method decreases

© 2018 The Authors. Published by Wiley-VCH Verlag GmbH & Co. KGaA, Weinheim

with an increase in the polarity of the solvent. According to these results, the stability of compound **2** increases on going from the gas phase to solution. The reported data also indicate that the dipole moment of product **2** in the gas phase (5.1575) is greater than the sum of the dipole moments of acetylacetone (1.5485) and the thiol (1.6140); this suggests that the electronic charge distribution of the product is highly asymmetric due to the presence of two fused heterocyclic rings and reaches the π system.

2.2.1.2. Electronic Spectra and TD-DFT Calculations

As reported in the previous section, the UV/Vis spectra of compounds **1** and **2** were obtained in chloroform, ethanol, and acetonitrile solutions to investigate the effects of the solvent on the molecular geometries and electronic structures of the studied compounds. The solution of **1** in chloroform showed three absorption bands at $\lambda_{max}=285.3$, 272.4, and 235.7 nm with $\varepsilon=3.437$, 3.4850, and 3.6943, respectively; the electronic absorption band of **1** in ethanol was observed at $\lambda_{max}=277.8$ nm with $\varepsilon=2.3998$, whereas the solution of compound **1** in acetonitrile showed different broad bands at $\lambda_{max}=297.6$, 285, 268.8, and 233.7 nm with $\varepsilon=3.2980$, 3.3616, 3.5475, and 3.6907, respectively. The electronic absorption spectra of the studied compounds in chloroform, ethanol, and acetonitrile were simulated by using TD-DFT calculations at the geometry optimized by using the B3LYP/6-311G(d,p) and 6-31++G(d,p) methods; for example, Figures 3, 4, and 5 represent the calculated electronic spectra of the studied compounds by using the 6-31++G (d,p) method.

The lowest energy electronic transition implies the transfer of an electron from the HOMO to the LUMO, and as such, we analyzed the first four excited states of the thiol and thione forms. The computed results calculated at the B3LYP/6-31++G(d,p) level, the excitation energies (*E*), absorption wavelengths (λ), and oscillator strengths (*f*) are depicted in Table S2. The oscillator strength is an important factor in measuring the intensity of an electronic transition assigned on the basis of the major contributions of the molecular orbitals. Electronic transitions for the thiol form were not affected by the polarity of the solvent used, and all of the electronic transitions were within nearly the same range in different solvents. Also, we observed that the second excited state with excitation energies of 4.531, 4.557, and 4.547 eV and oscillator strengths of 0.4046, 0.3769, and 0.3709 in chloroform, ethanol, and acetonitrile, respectively, corresponded mainly to the HOMO→LUMO+1 transition, which agrees with the experimental band at $\lambda=272.4$ nm. In contrast, the calculated electronic transitions of the thione form in different solvents were significantly affected by changing the solvent, and we found that the band observed at $\lambda=285$ nm in the UV/Vis spectrum was in harmony with that produced by TD-DFT calculations at $\lambda_{max}=300.57$, 286.72, and 282.93 nm in chloroform, ethanol, and acetonitrile, respectively; this band corresponds to the fourth excited state

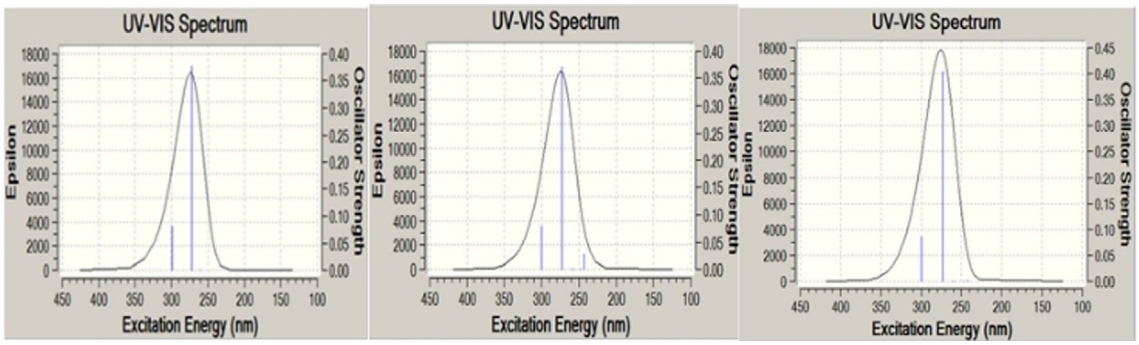

Figure 3. Calculated electronic spectra of thiol **1a** at TD-DFT 631++ in chloroform, ethanol, and acetonitrile (left to right).

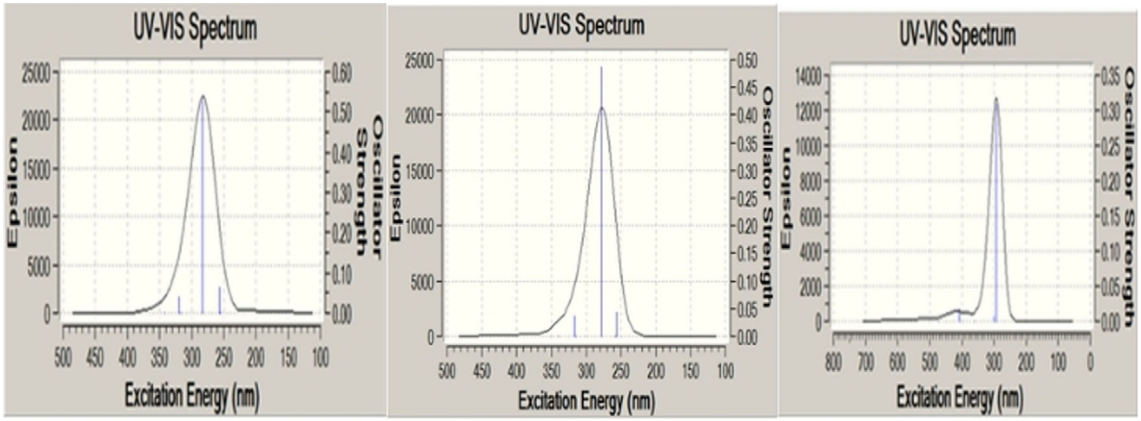

Figure 4. Calculated electronic spectra of thione **1b** at TD-DFT 631++ in chloroform, ethanol, and acetonitrile (left to right).

© 2018 The Authors. Published by Wiley-VCH Verlag GmbH & Co. KGaA, Weinheim

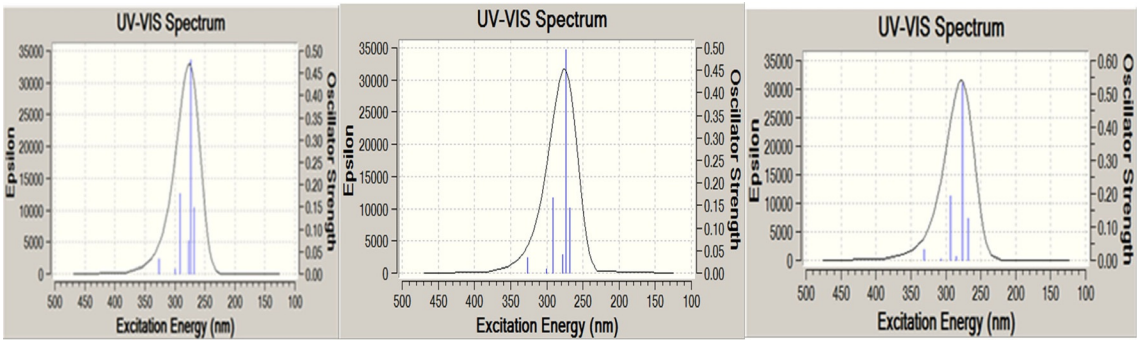

Figure 5. Calculated electronic spectra of quinazolinedione **2** at TD-DFT 631++ in chloroform, ethanol, and acetonitrile (left to right).

with excitation energies of 4.124, 4.324, and 4.382 eV and oscillator strengths 0.0057, 0.5268, and 0.5300 in chloroform, ethanol, and acetonitrile, respectively. This explains the orbital HOMO−2→LUMO transition in chloroform and the HOMO−1→LUMO and HOMO−1→LUMO+1 transitions in the case of ethanol with contributions of 14 and 67% respectively. Similarly, the contributions observed in the fourth excited state corresponded to the same orbital transitions in the case of acetonitrile, which may suggest a dominance of the thione form over the thiol form in chloroform and NH–SH tautomerism in polar solvents.

On the other hand, the electronic spectra of **2** showed different absorption maxima in different solvents. A solution of **2** in chloroform showed four bands at λ_{max} = 301.2, 285.3, 270.6, and 235.3 nm with ε = 3.4326, 3.5738, 3.6227, and 4.000, respectively. In ethanol, four bands at λ_{max} = 436.8, 354.9, 330.6, and 209.4 nm with ε = 0.1372, 0.3836, 0.4401, and 0.3131, respectively, were found. Finally, the UV/Vis spectrum of **2** in acetonitrile showed five absorption bands at λ_{max} = 299.1, 285, 269.1, 234.3, and 220.8 nm with ε = 3.3021, 3.3859, 3.5303, 3.6948, and 3.6733, respectively. To obtain accurate electronic transitions, TD-DFT-PCM calculations were performed on target compound **2**. By using B3LYP/6-31++G(d,p) and B3LYP/6-311G(d,p) to estimate the excited-state parameters, we could find an explanation for the basis-set effect of the different solvated media. The calculations in chloroform as a nonpolar solvent by using the 6-31++G(d,p) and B3LYP/6-311G(d,p) basis sets were nearly the same, but in the case of the polar solvents ethanol and acetonitrile, calculations with the 6-31++G(d,p) and B3LYP/6-311G(d,p) basis sets provided significantly different results. The TD-DFT-PCM results of quinazolinedione **2** in chloroform, ethanol, and acetonitrile with 31++G (d,p), and the excitation energies (*E*), absorption wavelengths (λ), and oscillator strengths (*f*) are depicted in Table S3. The results obtained with B3LYP/6-31++G(d,p) are very close to the experimental results. Six excited states were analyzed, and the dominant contribution to the maximum absorption for the first transition in all solvents was found to come from the HOMO→LUMO transition. Furthermore, in chloroform, the bands observed at λ = 301.2, 285.3, 270.6, and 235.3 nm were compared to the theoretical data of the third, fourth, fifth, and sixth excited states with oscillator strength of 0.1926 (HOMO−1→LUMO and HOMO→LUMO+1), 0.0103 (HOMO−1→LUMO), 0.5321, and 0.1235; the latter two bands were classified as a possible HOMO−2→LUMO+1 transition as a major contribution in chloroform. The theoretical data of the transitions in polar solvents (ethanol and acetonitrile) had nearly the same values of the calculated λ_{max} values in the six analyzed excited states. The band observed at λ_{max} = 277.8 nm in ethanol agreed with that at excited state four at λ_{max} = 277.77 nm with an oscillator strength of 0.0414 in EtOH, as well as the band at λ_{max} = 277.05 nm in CH_3CN with an oscillator strength of 0.0732, which represents a possible HOMO−1→LUMO transition. Also, the band observed at λ_{max} = 268.8 nm was compared to the theoretical band at λ_{max} = 267.87 nm in EtOH with an oscillator strength of 0.1437 and the band at λ_{max} = 267.96 nm with an oscillator strength of 0.1486, and they represent a possible HOMO−1→LUMO+1 transition.

2.2.2. Frontier Molecular Orbitals and Reactivity Parameters

The HOMO and LUMO represent the ability to denote and accept electrons.[31,32] These orbitals are termed frontier molecular orbitals (FMOs). The HOMO represents the ability to donate an electron, whereas the LUMO, as an electron acceptor, represents the ability to gain an electron. The energy gap between the HOMO and LUMO determines the energy that is very important to calculate the activation parameters,[33,34] and it can be used to describe further the chemical reactivity of the title compound and its precursor starting tautomer, as it is already known that the HOMO–LUMO energy gap (ΔE) is an important stability index.[35–37] As given in Table S4, the calculated electronic parameters, namely, ionization potential (IP), electron affinity (EA), hardness (η), and softness (σ), were calculated for the thione and thiol forms of the starting material and target product **2** in chloroform, ethanol, and acetonitrile. The IP and EA values were calculated as the negative energy eigen values of the HOMO and LUMO, respectively. Chemical hardness[38,39] was calculated according to Equation (1), whereas the global softness is the inverse of the global hardness [Eq. (2)].

$$\eta = \frac{(\mathrm{IP}-\mathrm{EA})}{2} \quad (1)$$

$$\sigma = \frac{1}{\eta} \quad (2)$$

© 2018 The Authors. Published by Wiley-VCH Verlag GmbH & Co. KGaA, Weinheim

The calculated values of these electronic parameters (Table S4) together with the results of the dipole moment values previously obtained (Table S1) confirmed that the polarity of the solvents played an important role in the reactivity and stability of the molecules (dipole moment of the thione form in the gas phase was found to be greater than that of the thiol form and increased upon increasing the dielectric constant of the solvent used). Also, the plots of the dipole moment of the thione form and the optimization step numbers gave a straight line with a negative slope in the gas phase and in ethanol and acetonitrile, whereas the relation in chloroform gave a straight line with a positive slope, which is the normal trend; this explains why compound **1** exists in the reactive thione form in chloroform, in which its hardness (η) is small and its softness (σ) is high.

The energy difference, known as the HOMO–LUMO gap, is an important chemical reactivity descriptor for molecular system. A small HOMO–LUMO gap corresponds to a chemically more reactive system and vice versa. The energy difference of the thiol form in the gas phase (4.8050 eV) is greater than that in chloroform (4.7799 eV), which is greater than that in ethanol (polar, protic solvent: 4.7680 eV), which is greater than that in acetonitrile (polar, aprotic solvent: 4.7669 eV); these results support the high reactivity of the thiol tautomer in polar solvents. On the other hand, solvent effects are also clearly shown with the thione form, for which $\Delta E = 4.1024$ eV in the gas phase and increases in polar solvents. This can be further seen from its hardness (η) and softness (σ) values in different solvents. A small η value is an indicator of the dominance of an electron-donating group in the molecular system. The σ parameter has opposite behavior to η, so that a high σ value is also an indicator of electron-donating groups.[40,41] As the results show in Table S4, the thione form has greater softness (σ) than the thiol form, with opposite results for the hardness (η); this reflects the role of the thione form as a good donor molecule in polar solvents and is in accordance with the experimental methods.

To evaluate the energetic behavior of the title compound, we performed calculations in chloroform, ethanol, and acetonitrile and in the gas phase. From the chemical parameters of studied product **2** by using the B3LYP/6-31++G(d,p) method, one concludes that the HOMO–LUMO gap of **2** is 4.1892 eV in the gas phase; upon increasing the dielectric constant (ε) of the solvent, the energy gap (ΔE) between the HOMO and LUMO slightly increases, and the values of the energy separation between the HOMO and LUMO are 4.4101, 4.4621, and 4.4681 eV in chloroform, ethanol, and acetonitrile, respectively. These energy gaps explain the charge-transfer interactions within the molecule and reveal a high stability of title compound **2** in polar solvents. This can also be observed from its hardness ($\eta = 2.205$, 2.231, and 2.231) and softness ($\sigma = 0.454$, 0.448, and 0.448) values in chloroform, ethanol, and acetonitrile, respectively.

The energies of the four important molecular orbitals of quinazoline dione **2**, that is, the second highest and highest occupied molecular orbitals (HOMO and HOMO−1) and the lowest and second lowest unoccupied molecular orbitals (LUMO and LUMO+1), were calculated by using B3LYP/6-31++G(d,p) and are presented in Figure 6. The plots show that the energy gap of the HOMO→LUMO explains the charge-transfer interaction within the molecule. This is clearly shown in the second lowest unoccupied orbit (LUMO+1), for which we find, in chloroform, electronic distribution over the whole molecule except for the *N*-phenyl ring, whereas the electronic distributions in ethanol and acetonitrile include the entire molecule. However, the electronic distributions in the other molecular orbitals (LUMO and LUMO+1) in all of the solvents are the same. This confirms the good stability of title compound **2** and that it has high chemical hardness.[42]

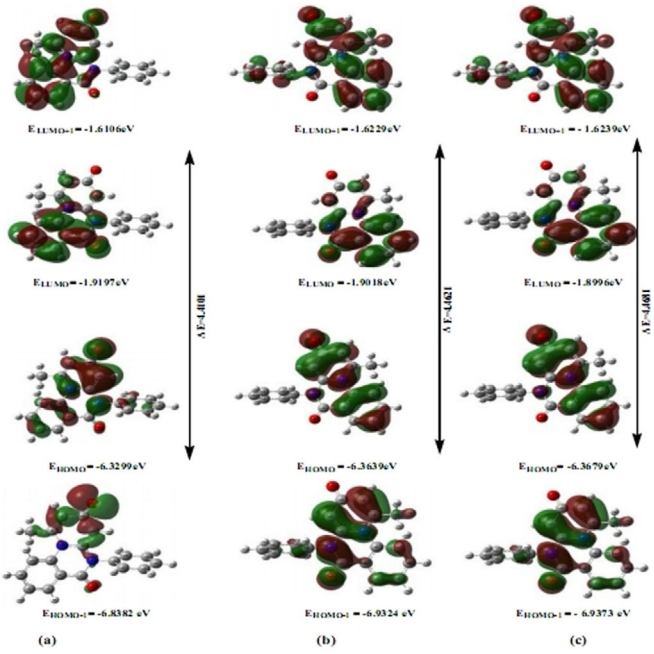

Figure 6. HOMO and LUMO of quinazolinedione **2** obtained in a) chloroform, b) ethanol, and c) acetonitrile.

The plots of the HOMO and LUMO computed by the B3LYP/6-optimized molecules in the gas phase are illustrated in Figure 7. The calculated energy gaps of quinazoline dione, acetylacetone, and the thiol form are 4.1892, 5.6268, and 4.8050 eV, respectively, and they reflect the chemical activity and stability of the molecules. The HOMO–LUMO transition implies transfer of electron density from SH of the thiol through the C–C group of acetylacetone; this can also be confirmed from the ionization potential of the system in the gas phase, as one observes that the IP of the thione form (6.3484 eV) is small relative to the IP of acetylacetone ($-E_{HOMO} = 7.0516$ eV), which supports the donating character of the thiol and the accepting character of acetylacetone. On the other hand, as a rule, charge transfer occurs if the energy gap between the HOMO of the donor and the LUMO of the acceptor is small; in the synthesis of title compound **2**, this value is equal to −4.68 eV, so it can be used in biological applications,[43,44] as it has a lower energy gap than the thione form and acetylacetone.

© 2018 The Authors. Published by Wiley-VCH Verlag GmbH & Co. KGaA, Weinheim

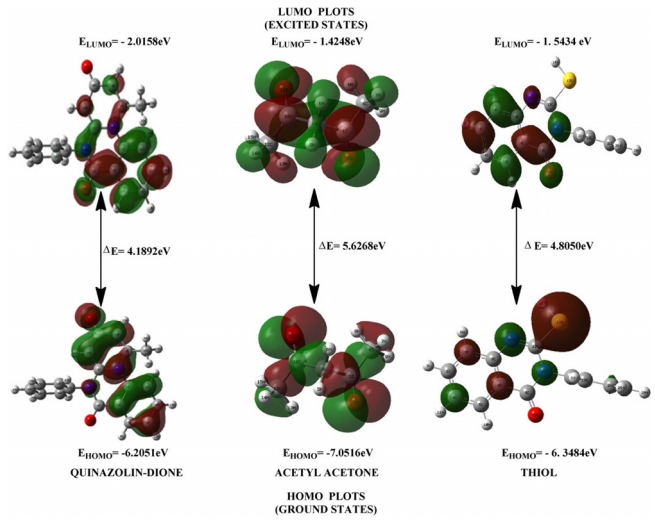

Figure 7. Energies of the HOMOs and LUMOs of quinazolinedione **2**, acetylacetone, and the thiol form in the gas phase.

2.2.3. Molecular Electrostatic Potential

The molecular electrostatic potential (MEP) surface is related to the electronic density, and it is a very useful descriptor in understanding sites for electrophilic attack and nucleophilic reactions, as well as hydrogen-bonding interactions; furthermore, it also provides a visual method to understand the relative polarity of a molecule.[45–47] To predict the electrophilic and nucleophilic reactive sites of the investigated molecule, the MEP at the B3LYP/6-31++G(d,p)-optimized geometry was calculated in the gas phase and in chloroform, ethanol, and acetonitrile. The MEP surface is represented by different colors, which increase in the order red < orange < yellow < green < blue. The negative (red and yellow) regions of the MEP are related to electrophilic reactivity, and the positive (blue) regions are related to nucleophilic reactivity (Figure 8).

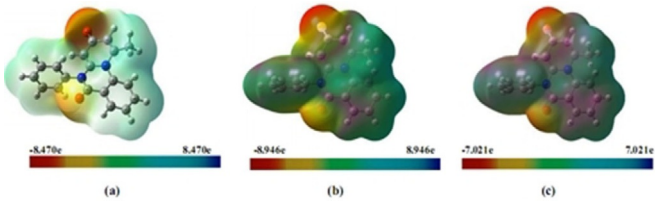

Figure 8. Molecular electrostatic potentials (MEPs) mapped on the electron density surface calculated at B3LYP/6-31++G(d,p) in a) chloroform and b) acetonitrile and c) in the gas phase.

Negative regions in studied molecule **2** in different solvents were found around both oxygen atoms of the quinazolinone and acetylacetone parts. The positive regions are localized on the nitrogen atoms, methyl group, and hydrogen atoms of the phenyl ring attached to the N atom of the quinazoline ring. These sites give information about the region from which the compound can have intermolecular interactions. Also, the darkness of the green color on the nitrogen atoms, methyl group, and the three carbon atoms of the newly formed ring of the product increases on going from chloroform, acetonitrile, and gas phase, that is, the color intensity varies from gas phase > acetonitrile > chloroform. The range of the color code of these maps is different according to the calculated phase, as shown in the figure.

2.2.4. Comparative Mulliken Charge and Geometric Parameters Analysis

Mulliken population analysis of the thiol and thione tautomers **1a** and **1b** and title compound **2** were computed by using B3LYP with the 6-31++G(d,p) and 6-311G(d,p) basis sets. The charge distributions of dipolar compounds are often altered significantly in the presence of a solvent reaction field. We examined the Mulliken atomic charges both in the gas phase and in solution. The results are shown in Tables S5–S7. The difference in the charge distributions is in accordance with the changes in the solvent polarity and basis-set effect, which play important roles in the changes in the Mulliken charges with the different basis sets. As expected, the charge distributions are influenced to some extent by a dielectric medium. In the case of thiol **1a**, a large degree of change is predicted upon increasing the dielectric constant of the solvent. The maximum change in charge significantly occurred upon using B3LYP with the 6-31++G(d,p) basis set only at O15, N16, and N17, which increased on going from the gas phase to acetonitrile solution just by 0.0847, 0.0802, and 0.0586 e, whereas upon using B3LYP with the 6-311G(d,p) basis set, an increase also occurred on going from the gas phase to acetonitrile solution just by 0.04596, 0.01058, and 0.0182 e at O15, N16, and N17, respectively. So, for the thiol form, the basis set and solvent effects have important influences on the changes in the Mulliken charges on O15, N16, and N17. On the other hand, the differences in the charge distributions in the cases of thione tautomer **1b** and title product **2** were affected by the previous factors (basis set and solvent effects), but in this case, the change in the charge occurred on most atoms of the segment, which is consistent with all other previous computational studies; this reflects the stability and reactivity of both composites. To compare the basis-set and solvent effects on the geometrical parameters, we performed geometry optimizations of the studied compounds at the B3LYP/6-31++G(d) and B3LYP/6-311G(d,p) levels in the gas phase and in chloroform, ethanol, and acetonitrile. The results of the geometrical bond lengths and bond angles of the studied compounds revealed no differences in either basis set. On the other hand, to see how solvation affected the geometry, we discuss, for example, only the geometry optimization of the studied compound using the PCM at the B3LYP/6-31++G(d) level. As shown in Figures S4–S15, solvation affects the geometrical parameters of thiol **1a** in the gas phase and in chloroform, ethanol, and acetonitrile, with a slight change in the bond length by 0.012–0.006 Å; as regards the bond angles of the thiol, only the H14–S13–C12 angle changes significantly, and it decreases on going from the gas phase to the solvent by 0.62°. The other bond angles do not change appreciably.

© 2018 The Authors. Published by Wiley-VCH Verlag GmbH & Co. KGaA, Weinheim

On the other hand, the bond angles of the thione form show an unexpected significant change for the structure calculated at the PCM at B3LYP/6-31++G(d) in chloroform, as we found that the C9–N15–C12, C3–N16–C12, and O14–C9–N15 angles decrease more than the others in the gas phase, ethanol, and acetonitrile by 1.18, 2.89, and 4.28°, respectively. The S13–C12–N16 and C4–C9–O14 angles increase by 1.74 and 5.91°, respectively, and consequently, the introduction of a solvent has a considerable effect on the geometry of the thione form. Product **2** is shown in the optimized geometrical, bond lengths and bond angles 631++G(d,p), and the values of the bond lengths and bond angles do not change.

2.2.5. NMR Spectral Analysis

The gauge-including atomic orbital (GIAO) ^{1}H NMR and ^{13}C NMR chemical shift calculations of compound **2** were made by the same method by using the 6-31++G(d,p) basis set in the gas phase and DMSO solution. The theoretical ^{1}H NMR and ^{13}C NMR chemical shifts were compared. The experimental and calculated chemical shifts of title compound **2** are presented in Table S8. In the ^{1}H NMR spectrum of the title compound, 4 main signals appear that integrate to 14 protons. In the experimental ^{1}H NMR spectrum, the chemical shifts of the aromatic protons are observed in the range of $\delta = 7.236$ to 7.961 ppm, which is typical for aromatic protons of organic molecules, whereas those calculated are between $\delta = 8.16$ and 9 ppm. The highest deviation of the experimental chemical shifts from the DFT-calculated values ($\delta_{calcd} - \delta_{exptl}$) is $\Delta\delta = 4.32$ ppm (H37); this can be attributed to the overestimated paramagnetic contribution in the DFT calculations. In the experimental ^{13}C NMR spectrum of quinazolinedione **2**, the aromatic carbon atoms give signals in overlapped areas of the spectrum with chemical shift values of $\delta = 100$ to 150 ppm;[48,49] similarly, chemical shifts are observed in the range of values calculated for C4 and C6, and therefore, the maximum deviations of the calculated chemical shifts from the experimental ones for C9/C29 and C3 ($\delta_{calcd} - \delta_{exptl}$) are $\Delta\delta = 12$ and 27 ppm, respectively. Deviations of the other carbon atoms range from $\Delta\delta = 3$ to 7 ppm. In general, the ^{1}H NMR spectroscopy experimental results correlate well with the values calculated at the DFT/6-31++G(d,p) level.

3. Conclusions

In this work,1-methyl-5-phenyl-5*H*-pyrido[1,2-*a*]quinazoline-3,6-dione (**2**) was synthesized from prepared 2-mercaptoquinazoline derivative **1**, and all the synthesized compounds were characterized by different techniques, including ^{1}H NMR spectroscopy, ^{13}C NMR spectroscopy, FTIR spectroscopy, UV/Vis spectroscopy, MS, and elemental analysis. UV/Vis spectroscopy data were calculated by using the DFT/B3LYP method with 6-311G(d,p) and 6-31++G(d,p) as two different basis sets in the gas phase and in chloroform, ethanol, and acetonitrile. The UV/Vis spectrum of the synthesized compound was studied by using the TD-DFT method, and the electronic transitions for various excited states were calculated and discussed. Spectral analyses and computational studies suggested the preference of compound **1** to exist in the thione form in the gas phase with NH–SH tautomerism in the solvated form. The experimental data and the computational calculations indicate that good correlation exists among these data. To predict the electrophilic and nucleophilic reactive sites of the product quinazoline dione **2**, the MEP at the optimized geometry was calculated in different media.

Experimental Section

General Methods

Melting points were taken in open capillary tubes by using a high-resolution Stuart SMP10 digital melting-point apparatus. Elemental analyses were performed at the Regional Center for Mycology and Biotechnology (RCMB), Al-Azhar University, Nasr city, Cairo, Egypt, by using a FLASH 2000 CHNS/O analyzer, Thermo Scientific. IR spectra were recorded by using potassium bromide disks with a PerkinElmer Spectrum RXI/FTIR System (Faculty of Pharmacy, Alexandria University, Egypt) and with a Bruker FTIR spectrometer Model:Tensor 37 (Faculty of Science, Alexandria University, Alexandria, Egypt) and are expressed in wavenumbers. Ultraviolet spectra were measured by using a PerkinElmer Lambada 4B UV/Vis (Faculty of Science, Alexandria University, Alexandria, Egypt). ^{1}H NMR and ^{13}C NMR spectra of the purified sample were determined in deuterated chloroform ($CDCl_3$) or deuterated dimethyl sulfoxide ([D_6]DMSO) with a JEOL JNM ECA 500 MHz NMR (Faculty of Science, Alexandria University, Egypt) or a Bruker AVANCE III Nano Bay 400 MHz FT-NMR spectrophotometer (Faculty of Pharmacy, Cairo University, Egypt). Chemical shifts are reported in δ as parts per million (ppm) downfield from tetramethylsilane as an internal standard. Mass spectrometry was performed with a direct inlet part to mass analyzer in a Thermo Scientific GCMS model ISQ (70 eV EI mode). Also, elemental analysis was performed with a Thermo Finnigan Flash EA microanalyzer, both at the Regional Center for Mycology and Biotechnology (RCMB), Al-Azhar University, Nasr city, Cairo, Egypt. Reaction progress was monitored by thin-layer chromatography (TLC) by using flexible sheets 7.5×2.5 (Baker-flex) silica gel IB-F (J. T. Baker Chemical CO, west Germany); chloroform or chloroform/ethanol (9:1) was used as the eluting system to examine compound purity and reaction completion. The spots were visualized by using a Vilber Lourmat ultraviolet lamp at $\lambda = 365$ and 254 nm.

Synthesis

2-Mercapto-3-phenyl-2,3-dihydro-1*H*-quinazolin-4-one (**1**): A mixture of equimolar amounts of phenylthiourea (15.2 g, 10 mmol) and anthranilic acid (13.7 g, 10 mmol) was fused together for 4 h in a round-bottomed flask provided with an air condenser and heated in an oil bath at 175–180 °C and was then cooled and added to cold water (40 mL). The solid product obtained was collected and recrystallized from ethanol to give **1** (70%): m.p. >297 °C (as reported in ref. [50]: >300 °C); ^{1}H NMR (500 MHz, [D_6]DMSO): $\delta = 9.98$ (s, 1H, NH, exchangeable), 6.64–7.70 (m, 9H, ArH), 5.45 ppm (s, 1H, SH, exchangeable); ^{13}C NMR (500 MHz, [D_6]DMSO): $\delta = 179$ (C2, CS), 165 (C4, CO), 138 (C9, C11), 132 (C7), 130 (C10), 128 (C13, C15), 127 (C5), 125 (C8), 124 (C6, C14), 120 ppm (C12, C16); IR (KBr): $\tilde{\nu} = 3245$ (NH), 2924 (SH), 1661 (CO), 1621 (CN), 1531 (C=C), 1268 cm^{-1}(CS); elemental analysis calcd (%)

© 2018 The Authors. Published by Wiley-VCH Verlag GmbH & Co. KGaA, Weinheim

for $C_{14}H_{10}N_2OS$ (254.31): C 66.12, H 3.96, N 11.02, S 12.61%; found: C 67.56, H 3.16, N 10.20, S 12.91.

1-Methyl-5-phenyl-5*H*-pyrido[1,2-*a*]quinazoline-3,6-dione (**2**): Acetylacetone (10 mmol) was added to a solution of sodium ethoxide in ethanol (0.56 g of sodium in 50 mL ethanol), and the mixture was stirred for 2 h. Compound **1** (4.1 g, 10 mmol) was added. The mixture was heated under reflux for 5 h. Ethanol was removed under reduced pressure, and the residue was poured into cold water (100 mL) and extracted with ether. The extracted solvent was dried with anhydrous sodium sulfate and was removed under reduced pressure to give **2** (80%): m.p. 268–270 °C; ^{1}H NMR (500 MHz, [D_6]DMSO): δ = 7.236–7.961 (m, 9H, ArH), 3.687 (s, 3H, CH_3), 2.510 ppm (s, 2H, CHCOCH); ^{13}C NMR (500 MHz, [D_6]DMSO): δ = 163 (C6), 156 (C30), 142 (C4, C2), 138 (C17), 132 (C10), 128 (C7, C-2, C28), 124 (C24), 120 (C18, C19), 117 (C9, C5), 112 (C11), 99 (C3), 92 (C29), 64.5 (C1), 22 ppm (C32); IR (KBr): $\tilde{\nu}$ = 1663, (CO), 1529 cm^{-1} (C=C); MS (EI): *m/z* (%): 272 (16.64), 270 (14.92), 257 (12.50), 255 (16.69), 254 (68.52), 253 (100), 236 (1.02), 221 (2.05), 196 (1.30), 161 (2.92), 145 (4.29), 133 (2.75), 127 (2.65), 118 (10.75), 102 (4.43), 91 (6.96), 76 (13.80), 55 (2.03), 43 (6.44); elemental analysis calcd (%) for $C_{19}H_{14}N_2O_2$ (302): C 75.50, H 4.64, N 9.27%; found: C 74.70, H 4.57, N 9.99.

Computational Methods

All calculations for the studied compounds were performed by using the Gaussian 09 software package[51] with a Pentium IV processor personal computer. The calculations were performed by DFT by using the Becke's three parameter exchange functional[52] with a hybrid functional by means of the Lee, Yang, and Parr (LYP) correlation functional[53] B3LYP method. Energy optimization of the ground states of the compounds was performed by using the split-valence double zeta basis sets 6-31++G and 6311G with two polarized basis functions (d and p), for which the p-type orbital was added to all hydrogen atoms as well as a diffuse function. The origin of the electronic spectra was computed by using the time-dependent DFT (TD-DFT) method at the same level of the theory. The gas-phase-optimized structure of the most stable isomer was thus classified as its starting geometry; complete geometry optimization without restriction was performed in DMSO as the solvent used to predict the ^{1}H NMR spectra of the studied compounds. The ^{1}H NMR chemical shifts were calculated with the gauge-independent atomic orbital (GIAO) approach with the B3LYP/6311G basis set. The effect of solvent during TD-DFT analysis was considered by the polarizable continuum model (PCM) of Tomasi and coworkers.[54] The geometries were optimized by minimizing the energies with respect to all geometrical parameters. Gauss-View and Chem craft programs[55] were used to get computation results and to visualize the optimization structures and to draw the frontier molecular orbital (FMOs) and molecular electrostatic potential (MEP) maps.[56]

Conflict of Interest

The authors declare no conflict of interest.

Keywords: electrostatic potential · density functional calculations · dipole moment · nitrogen heterocycles · solvent effects

[1] M. A. Aziza, M. W. Nassar, S. G. Abdel-Hamide, A. E. El-Hakim, A. S. El Azab, *Ind. J. Heterocycl. Chem.* **1996**, *6*, 25–30.
[2] V. J. Ram, B. K. Tripathi, A. K. Srivastava, *Bioorg. Med. Chem.* **2003**, *11*, 2439–2444.
[3] D. M. Purohit, V. R. Bhuva, V. H. Shah, *Chemistry (Rajkot, India).* **2003**, *1*, 233–245.
[4] a) P. Rani, V. Archana, K. Srivastava, A. Kumar, *Ind. J. Heterocycl. Chem.* **2002**, *41B*, 2642–2646; b) V. Alagarsamy, V. Muthukumar, N. Pavalarani, P. Vasanthanathan, R. Revathi, *Biol. Pharm. Bull.* **2003**, *26*, 557–559.
[5] O. Guiping, Z. Peiquan, Xu. Gangfang, S. Baoan, Y. Song, J. Linhong, X. Wei, H. Deyu, L. Ping, C. Zhuo, *Molecules* **2006**, *11*, 383–392.
[6] A. M. Alafeefy, *J. Saudi Chem. Soc.* **2011**, *15*, 337–343.
[7] A. K. Nanda, S. Ganguli, R. Chakraborty, *Molecules* **2007**, *12*, 2413–2426.
[8] P. Mani Chandrika, T. Yakaiah, A. Raghu Ram Rao, B. Narsaiah, N. ChakraReddy, V. Sridhar, J. Venkateshwara Rao, *Eur. J. Med. Chem.* **2007**, *42*, 147–152.
[9] S. Tripti, S. Sharma, V. K. Srivastava, A. Kumar, *Ind. J. Chem.* **2006**, *45B*, 2558–2565.
[10] K. N. Venugopala, S. K. Nayak, R. l M. Gleiser, M. E. Sanchez-Borzone, D. A. Garcia, B. Odhav, *Chem. Biol. Drug Des.* **2016**, *88*, 88–96.
[11] X. Liu, R. Q. Huang, Z. Yang, *Chin. J. Appl. Chem.* **1999**, *16*, 23–26.
[12] G. Fitzgerald, J. Andzelm, *J. Phys. Chem.* **1991**, *95*, 10531–10534.
[13] T. Ziegler, *Pure Appl. Chem.* **1991**, *63*, 873–880.
[14] J. Andzelm, E. Wimmer, *J. Chem. Phys.* **1992**, *96*, 1280–1303.
[15] G. E. Scuseria, *J. Chem. Phys.* **1992**, *97*, 7528–7530.
[16] R. M. Dickson, A. D. Becke, *J. Chem. Phys.* **1993**, *99*, 3898–3905.
[17] B. G. Johnson, P. M. W. Gill, J. A. Pople, *J. Chem. Phys.* **1993**, *98*, 5612–5626.
[18] N. Oliphant, R. J. Bartlett, *J. Chem. Phys.* **1994**, *100*, 6550–6556.
[19] V. N. Nemykin, J. G. Olsen, E. Perera, P. Basu, *Inorg. Chem.* **2006**, *45*, 3557–3568.
[20] G. Menconi, N. Kaltsoyannis, *Chem. Phys. Lett.* **2005**, *415*, 64–68.
[21] S. Prasad, S. Ash, A. Misra, S. Dalai, *THEOCHEM.* **2007**, *807*, 33–41.
[22] K. Zborowski, A. Korenova, M. Uher, L. M. Proniewicz, *J. Mol. Struct.* **2004**, *683*, 15–23.
[23] W. P. Oziminski, J. C. Dobrovolski, A. P. Mazurek, *J. Mol. Struct.* **2004**, *680*, 107–115.
[24] T. J. Dines, H. Onoh, *Spectrochim. Acta.* **2006**, *A64*, 891–900.
[25] S. Ozturk, M. Akkurt, A. Cansiz, M. Koparir, M. Sekerci, F. W. Heinemann, *Acta Crystallogr. Sect. E* **2004**, *60*, o425–o427.
[26] S. Ozturk, M. Akkurt, A. Cansiz, M. Koparir, M. Sekerci, F. W. Heinemann, *Acta Crystallogr. Sect. E* **2004**, *60*, o642–644.
[27] J. S. Kwiatkowski, T. J. Zielenski, R. Rein, *Adv. Quantum Chem.* **1986**, *18*, 85–130.
[28] A. Masternak, G. Wenska, J. Milecki, B. Skalski, S. Franzen, *J. Phys. Chem.* **2005**, *109*, 759–766.
[29] Y. Le, J. F. Chen, M. Pu, *Int. J. Pharm.* **2008**, *358*, 214–218.
[30] M. Koparir, C. Orek, P. Koparir, K. Sarac, *Spectrochim. Acta Part A* **2013**, *105*, 522–531.
[31] S. Subashchandrabose, A. R. Krishnan, H. Saleem, V. Thanikachalam, G. Manikandan, Y. Erdogdu, *J. Mol. Struct.* **2010**, *981*, 59–70.
[32] D. Shoba, S. Periandy, M. Govindarajan, P. Gayathri, *Spectrochim. Acta Part A* **2015**, *136*, 852–863.
[33] I. Fleming, *Frontier Orbitals and Organic Chemical Reactions*, Wiley, London, **1976**.
[34] A. M. Asiri, M. Karabacak, M. Kurt, K. A. Alamry, *Spectrochim. Acta Part A* **2011**, *82*, 444–455.
[35] M. Rocha, A. Di Santo, J. M. Arias, D. M. Gil, A. B. Altabef, *Spectrochim. Acta Part A* **2015**, *136*, 635–643.
[36] M. Amalanathan, V. K. Rastogi, I. H. Joe, M. A. Palafox, R. Tomar, *Spectrochim. Acta Part A* **2011**, *78*, 1437–1444.
[37] R. G. Parr, Y. Weitao, *Density-Functional Theory of Atoms and Molecules (International Series of Monographs on Chemistry)*, Oxford University Press, New York, **1989**.
[38] W. Yang, R. G. Parr, *Proc. Natl. Acad. Sci. USA* **1985**, *82*, 6723–6726.
[39] F. Cuenú, J. Londono-Salazar, J. E. Torres, R. Abonia, R. F. D'Vries, *J. Mol. Struct.* **2018**, *1152*, 163–176.
[40] R. G. Parr, R. G. Pearson, *J. Am. Chem. Soc.* **1983**, *105*, 7512–7516.
[41] O. Tamer, B. S. Arslan, D. Avcı, M. Nebioğlu, Y. Atalay, B. Çoşut, *J. Mol. Struct.* **2016**, *1106*, 89–97.
[42] S. Muthu, S. Renuga, *Spectrochim. Acta Part A* **2014**, *118*, 683–694.

 © 2018 The Authors. Published by Wiley-VCH Verlag GmbH & Co. KGaA, Weinheim

[43] A. K. Srivastava, N. Misra, *Can. J. Chem.* **2014**, *92*, 234 – 239.
[44] A. K. Srivastava, A. K. Pandey, S. Jain, N. Misra, *Spectrochim. Acta Part A* **2015**, *136*, 682 – 689.
[45] J. Zevallos, A. Toro-Labbe, *J. Chil. Chem. Soc.* **2003**, *48*, 39 – 47.
[46] M. Ozdemir, M. Sonmez, F. Sen, M. Dincer, N. Ozdemir, *Spectrochim. Acta Part A* **2015**, *137*, 1304 – 1314.
[47] V. Balachandran, M. Murugan, V. Karpagam, M. Karnan, G. Ilango, *Spectrochim. Acta Part A.* **2014**, *130*, 367 – 375.
[48] K. Pihlaja, E. Kleinpeter, *Carbon-13 NMR Chemical Shifts in Structural and Stereochemical Analysis*, VCH Publishers, New York, **1994**.
[49] H.-O. Kalinowski, S. Berger, S. Braun, *Carbon-13 NMR Spectroscopy*, Wiley, Chichester, **1988**.
[50] N. N. Vereshchagina, Ya. Postovskii, *Zh. Obshch. Khim.* **1964**, *34*, 1745 – 1748; *Chem. Abstr.* **1964**, *60*, 1743c.
[51] Gaussian 09, Revision A.02, M. J. Frisch, G. W. Trucks, H. B. Schlegel, G. E. Scuseria, M. A. Robb, J. R. Cheeseman, G. Scalmani, V. Barone, G. A. Petersson, H. Nakatsuji, X. Li, M. Caricato, A. Marenich, J. Bloino, B. G. Janesko, R. Gomperts, B. Mennucci, H. P. Hratchian, J. V. Ortiz, A. F. Izmaylov, J. L. Sonnenberg, D. Williams-Young, F. Ding, F. Lipparini, F. Egidi, J. Goings, B. Peng, A. Petrone, T. Henderson, D. Ranasinghe, V. G. Zakrzewski, J. Gao, N. Rega, G. Zheng, W. Liang, M. Hada, M. Ehara, K. Toyota, R. Fukuda, J. Hasegawa, M. Ishida, T. Nakajima, Y. Honda, O. Kitao, H. Nakai, T. Vreven, K. Throssell, J. A. Montgomery, Jr., J. E. Peralta, F. Ogliaro, M. Bearpark, J. J. Heyd, E. Brothers, K. N. Kudin, V. N. Staroverov, T. Keith, R. Kobayashi, J. Normand, K. Raghavachari, A. Rendell, J. C. Burant, S. S. Iyengar, J. Tomasi, M. Cossi, J. M. Millam, M. Klene, C. Adamo, R. Cammi, J. W. Ochterski, R. L. Martin, K. Morokuma, O. Farkas, J. B. Foresman, D. J. Fox, Gaussian, Inc., Wallingford, CT, **2009**.
[52] A. D. Becke, *J. Chem. Phys.* **1993**, *98*, 5648 – 5652.
[53] C. Lee, W. Yang, R. G. Parr, *Phys. Rev.* **1988**, *B37*, 785 – 789.
[54] V. Barone, M. Cossi, J. Tomasi, *J. Chem. Phys.* **1997**, *107*, 3210 – 3221.
[55] G. A. Zhurko, D. A. Zhurko, *Chemcraft: Lite Version Build 08* (Freeware), **2005**.
[56] J. S. Murray, K. D. Sen (Eds.), *Molecular Electrostatic Potentials: Concepts and Applications (Theoretical and Computational Chemistry)*, Elsevier, Amsterdam, **1996**, Vol. 3.

Received: July 17, 2018

 © 2018 The Authors. Published by Wiley-VCH Verlag GmbH & Co. KGaA, Weinheim